IEEE Photonics Journal
An IEEE Photonics Society Publication

Open Access

Red Shift of Side-Polished Fiber Surface Plasmon Resonance Sensors With Silver Coating and Inhibition by Gold Plating

Volume 9, Number 3, June 2017

Mingquan Li
Zhiyong Bai
Feng Zhang
Maoxiang Hou
Ying Wang
Changrui Liao
Wei Jin
Yiping Wang

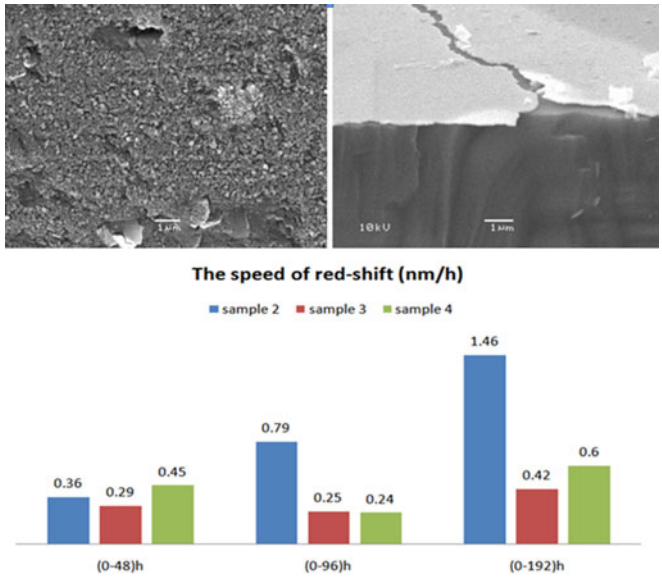

DOI: 10.1109/JPHOT.2017.2702193
1943-0655 © 2017 IEEE

Red Shift of Side-Polished Fiber Surface Plasmon Resonance Sensors With Silver Coating and Inhibition by Gold Plating

Mingquan Li,[1] Zhiyong Bai,[1] Feng Zhang,[1] Maoxiang Hou,[1] Ying Wang,[1] Changrui Liao,[1] Wei Jin,[2] and Yiping Wang[1]

[1]Key Laboratory of Optoelectronic Devices and Systems of Ministry of Education and Guangdong Province, College of Optoelectronic Engineering, Shenzhen University, Shenzhen 518060, China
[2]Department of Electrical Engineering, The Hong Kong Polytechnic University, Hong Kong

DOI:10.1109/JPHOT.2017.2702193

Manuscript received March 25, 2017; revised April 28, 2017; accepted May 3, 2017. Date of publication May 18, 2017; date of current version May 25, 2017. This work was supported in part by the National Natural Science Foundation of China under Grant 61605123, Grant 61425007, Grant 61377090, and Grant 61575128; in part by the China Postdoctoral Science Foundation under Grant 2015M582406 and Grant 2016M008547; in part by the Guangdong Science and Technology Department under Grant 2014A030308007, Grant 2014B050504010, Grant 2015B010105007, and Grant 2015A030313541; in part by the Science and Technology Innovation Commission of Shenzhen under Grant ZDSYS20140430164957664, Grant GJHZ20150313093755757, Grant KQCX20140512172532195, and Grant JCYJ20150324141711576; and in part by the Pearl River Scholar Fellowships under Grant JCYJ20150324141711576. Corresponding author: Yiping Wang (e-mail: ypwang@szu.edu.cn).

Abstract: The degeneration of Ag coatings on the polished surfaces of side-polished fibers (SPFs) with different surface topographies, and its inhibition by Au plating were studied by the time-dependent red shift of the resonance wavelength of SPF surface plasmon resonance (SPR) sensors. The surface topography determines the Ag-particle distribution, and affects the optical performance. The resonance wavelength of rough and smooth samples demonstrates a red shift over time. However, the service lifetime of an Ag-SPR sensor with a rough surface is less than 48 h because an abundance of coating flakes destroys the integrity of the Ag coating, and accelerates oxidation. Degeneration does not decrease its sensitivity. The smooth surface retards the degeneration rate. A thin Au plating decreases the resonance bandwidth for the rough surface, and provides a resonance wavelength near the middle of the ideal range between 533 and 620 nm. The position of the resonance wavelength can be adjusted by changing the proportions of Ag and Au in the compound coating. The Au plating retards the rate of Ag degeneration, where the maximum degeneration rate of a pure Ag coating is 3.5 times greater that of an Ag–Au compound coating between 96 and 192 h.

Index Terms: Side-polished fiber (SPF), surface plasmon resonance (SPR), silver coating, silver–gold compound coating, degeneration.

1. Introduction

Over the past two decades, numerous types of optical sensors have been proposed based on surface plasmon resonance (SPR) and applied to a wide range of chemical and biological sensing tasks. Because of limitations in Kretschmann prism geometry [1]–[3], e.g., the large size and

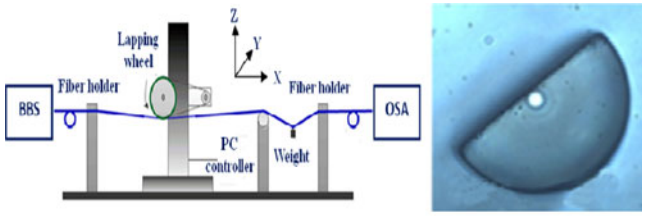

Fig. 1. Schematic of the wheel polishing apparatus and the cross section of a side-polishing fiber.

cumbersome packaging, sensors utilizing the SPR phenomenon have been developed based on optical interaction effects which employ alternative structures such as optical fibers. SPR-based sensors which utilize optical fibers (hereafter denoted simply as fiber SPR sensors) offer some unique advantages, such as easy coupling, remote sensing, immunity to electromagnetic interference, fast response rates, and a high potential for miniaturization [4], [5]. Presently, fiber SPR sensors based on side-polished fibers (SPFs) have attracted increasing attention owing to their relatively simple fabrication. They have served as a wide variety of optical components including polarizers, resonators, switches, and evanescent fiber sensors [6]–[9].

Most SPFs are obtained by a polishing method that uses various fixtures such as V-shaped groove polishing wheels or direct polishing wheels. Regardless of the precise polishing method used, the working surface through which the evanescent field penetrates, inevitably exhibits surface irregularities that are typical of machined surfaces. Such surface irregularities can have profound effects on optical performance. Zhao *et al.* [10] demonstrated that a rough SPF surface (as opposed to a smooth surface, which induces a high contrast interference spectrum) can be used directly as a promising sensing device for detecting temperature and strain. However, the author did not discuss the influence of the surface topography on the refractive index detection performance of the SPF sensor. The use of an SPF with a noble-metal coating as a refractive index detector is one of the most important applications in biochemistry. Silver is inexpensive and its SPR coupling performance is better than Au; however, biochemical applications use Au films rather than Ag films because of the rapid oxidation of Ag in air, particularly in humid environments [11]–[13]. Minimal literature exists on the effect of Ag film degradation on the performance of Ag-SPR sensors.

For studying deeply the effect of Ag film degradation on different SPF surfaces, we use experimental methods to investigate the influence of Ag coating degeneration on the optical performance of SPF sensors with different surface topographies. The effectiveness of a thin Au plating in inhibiting Ag-coating degeneration was investigated. This study is expected to contribute significantly to the optimization of polishing conditions, and to an improved performance of optical fiber Ag-SPR sensors based on SPFs.

2. Experimental Details

2.1 Fabrication of SPFs With Different Surface Topographies

SPFs were fabricated by using a wheel polishing machine (WanRun Ltd., WuXi, China) for experimental testing. Fig. 1(a) illustrates the processing and optical transmission analysis setup used. The polishing parameters used for the various samples evaluated are listed in Table 1. The fiber was a standard single-mode fiber (SMF; Corning SMF-28) with a core/cladding diameter of 8.2/125 μm. A broadband light source with a range of 1250 nm to 1650 nm and an optical spectrum analyzer (OSA; Yokogawa AQ6370C) were used to measure the transmission profile of the SPF during the polishing process. The residual thickness of the SPF was evaluated preliminarily by optical microscopy. Because of fluctuations in the polished surface, the precise thickness was evaluated by OSA according to the transmission loss. The length of polished section are 5 mm for all the samples. Fig. 1(b) presents an optical microscopy image of a fiber cross section after polishing.

TABLE 1
Polishing Parameters for Side-Polished Fiber Fabrication

Sample	Wheel speed (rpm)	Wheel moving feed rate (mm/min)	Abrasive Grading (#)	Thickness of cladding (dB)	Wheel Radius (mm)	Polishing Fluid	Environment	
							Temperature (°C)	Relative humidity (%)
1	800	1000	1500	−1	100	Paroline	25	40
2			10000	−1				
3			1500	−1				
4			10000	−1				

Note: SPF surfaces are directly related to the size of abrasive structures employed in the polishing process. Generally, larger grading # (i.e. smaller abrasive particles) of abrasive paper leads to smoother surface/smaller surface roughness of the fiber.

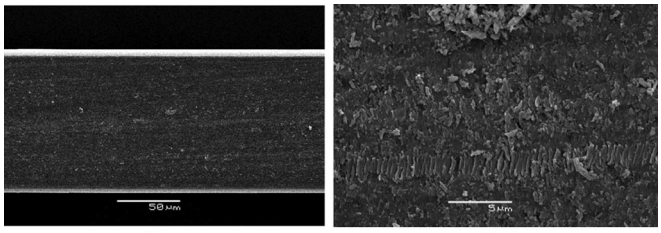

(a) (b)

Fig. 2. SEM images of an SPF (sample 1) polished by 1500# abrasive paper. (a) 50 × magnification. (b) 5000 × magnification.

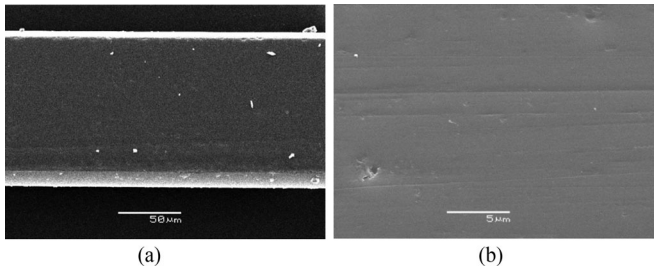

(a) (b)

Fig. 3. SEM images of an SPF (sample 2) polished by 10000# abrasive paper. (a) 50 × magnification. (b) 5000 × magnification.

Figs. 2 and 3 present scanning electron microscopy (SEM) images for different surfaces polished by using 1500# and 10000# abrasive papers, respectively. By comparing Figs. 2 and 3, we can see that the surface topography of the two samples exhibits obvious differences. The coarse abrasive induces numerous fractures and scratches, and waviness across the fiber axis. The fine abrasive tends to produce a smooth surface with little debris and minor pitting. The two surface profiles result from the different material removal mechanisms. The fine abrasive tends to remove SiO_2 by a plastic mechanism, and the coarse abrasive produces a brittle surface with a high amplitude of surface fluctuation. When coating the polished fiber surface with a metal film to fabricate an SPR sensor, the basic topography will have an important influence on the optical performance of the resulting sensor. The effect of the different surface topographies on the structure of the Ag film will affect the oxidation properties of the Ag coatings, which, in turn, will affect the sensor performance

TABLE 2
Coating Parameters for Side-Polished Fibers

Sample	Thickness of Ag film (nm)	Thickness of Au film (nm)	Total Thickness (nm)	Cleaning Fluid	Environment*	
					Temperature (°C)	Relative humidity (%)
1	45	0	45	Ethyl alcohol	25	40
2	45	0	45			
3	40	5	45			
4	40	5	45			

*During storage and testing.

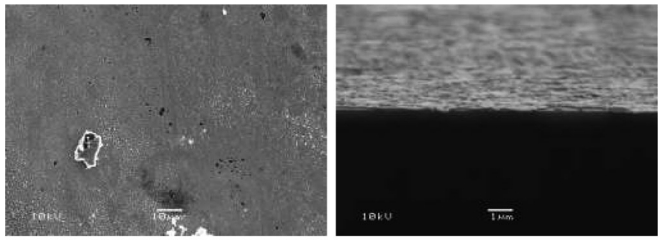

(a) (b)

Fig. 4. SEM images of Ag-coated SPF. (a) Surface. (b) Profile.

From Fig. 3, we can determine that different surface topographies produce different effects on the transmission loss and spectrum shape of the transmitted light signals. The figure also indicates that transmission loss is greatest at longer wavelengths for both samples. The coarse abrasive paper tends to induce a greater loss than the smooth abrasive paper for equivalent residual cladding thicknesses. This leads to a highly variable transmission spectrum, which may influence the formation of SPR waves and lead to difficulty in evaluating SPR decreases.

2.2 Coating and Detection of SPR Effect

Vacuum thermal evaporation was used to deposit Ag films with a uniform thickness over the SPFs. The coating machine used (SKY Technology Development Co., Ltd.) measures continuously and controls the thickness of the film using a crystal oscillator. The evaporation material was Ag particles of high purity (99%), and the vacuum pressure was set at 5×10^{-5} Pa. The evaporation speed was controlled to $\sim$4 nm/s by adjusting the electric-heater current. The detailed coating parameters for the various samples evaluated are listed in Table 2.

Figs. 4 and 5, respectively, present SEM images for an Ag film and an Ag–Au compound film deposited simultaneously on a silicon wafer when fabricating the SPF samples to observe the coating characteristics and to measure the coating thickness. By comparing Figs. 4 and 5, we observe that the Ag film is not as well formed as the Ag–Au compound film. The Ag film presents numerous voids on the surface, large debris, and local surface irregularities, which may be one of the causes of Ag-film degeneration. The Ag film can be shielded from the surrounding environment by plating with Au, and, theoretically, inhibit the degeneration of the Ag film. However, the compound film also has its own defects, such as a large crack because of stress between the different materials, as shown in Fig. 5(b), which would be expected to diminish the inhibition effect. The thicknesses of

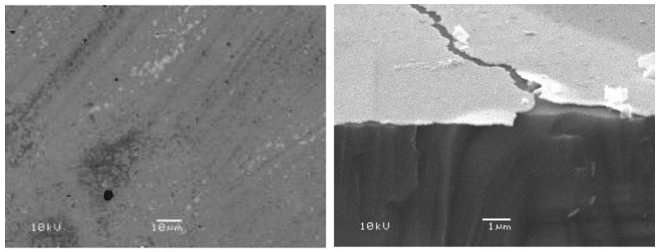

Fig. 5. SEM images of SPF with Ag-Au compound coating. (a) Surface. (b) Profile.

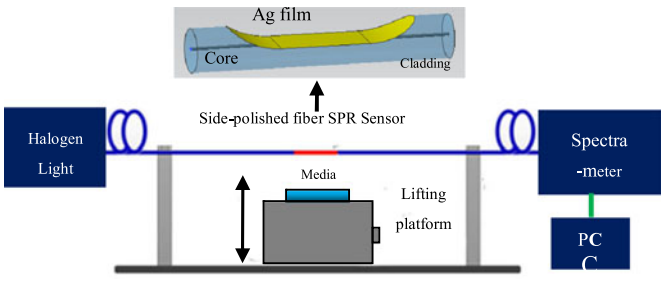

Fig. 6. Testing system to obtain the refractive index response of SPF sensors.

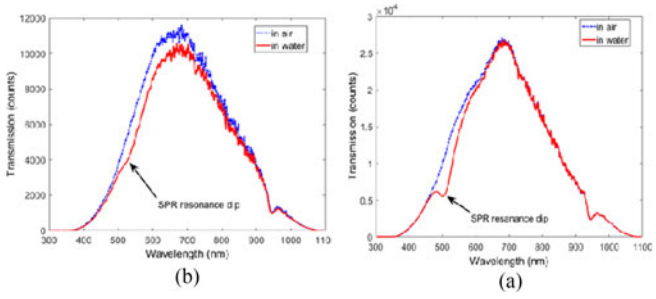

Fig. 7. Transmission spectra of Ag-coated SPF sensors. (a) Sample 1 (1500# abrasive paper). (b) Sample 2 (10000# abrasive paper).

the Ag films (samples 1 and 2) are ~49.5 nm, and those of the compound films (samples 3 and 4, respectively) are ~50.2 nm, as obtained by a Form Talysurf (Taylor Hobson) surface profiler.

The testing system in Fig. 6 was used to study the response characteristics of SPF sensors with different films to the refractive index of a surrounding medium. The platform consisted mainly of a halogen lamp light source (Ocean Optics, LS-3000, 300–1100 nm), optical fiber spectrometer (Ocean Optics, QE65000, 200–1100 nm), personal computer, manual lifting platform, and optical fiber fixture devices. The media used were standard refractive index liquids. The environmental temperature and humidity during storage and testing are listed in Table 2.

3. Results and Discussion

3.1 Degeneration of Ag Coatings Applied to Rough and Smooth Polished Surfaces

Fig. 7(a) and (b) presents the transmission spectra of samples 1 and 2, respectively, in different media (air and water). As shown in Fig. 7(b), comparing the transmission spectrum in air with that in water demonstrates the SPR resonance absorption effect. Under a condition of phase matching, the transmission spectrum distributes over a particular wavelength range, escapes the evanescent

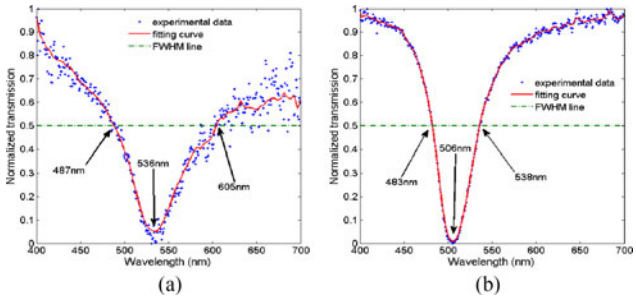

Fig. 8. Normalized transmission spectra of Ag-coated SPF sensors. (a) Sample 1 (1500# abrasive paper). (b) Sample 2 (10000# abrasive paper).

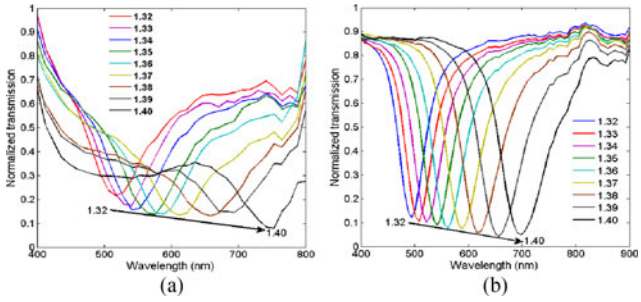

Fig. 9. Normalized transmission spectra of Ag-coated SPF sensors in different refractive index media. (a) Sample 1 (1500# abrasive paper). (b) Sample 2 (10000# abrasive paper).

field, and couples to the SPW of the Ag coating. In Fig. 7(a), the resonance dip is not very clear, but the absorption bandwidth is greater than that shown in Fig. 7(b). The coarse abrasive tends to broaden the resonance bandwidth and, thus, reduces the spectrum contrast at the resonance wavelength.

Fig. 8(a) and (b) shows the normalized spectra of Fig. 7(a) and (b), respectively. The resonance wavelengths of samples 1 and 2 are 536 nm and 506 nm, respectively. Compared with the ideal position of 533 nm that would result from an ideal flat surface, the resonance dip of sample 1 demonstrates a slight red shift, and that of sample 2 demonstrates a substantial blue shift. This phenomenon occurs because of the differing surface topographies of the polished surfaces, where the fine polished surface induces a blue shift in the resonance wavelength and the coarse polished surface induces a red shift. The full width at half maximum (FWHM) values of the normalized spectra for samples 1 and 2 are 118 nm and 56 nm, respectively. This broadening effect is visible in Fig. 7(a). The coarse abrasive tends to induce a larger FWHM, which is also an important parameter of sensor quality.

To study the index of refraction sensitivity of SPFs with different surface topographies, all samples were immersed in standard refractive index matching fluids, and the normalized transmission spectra are given in Fig. 9. Fig. 9 shows that the resonance wavelength shifts toward longer wavelengths, and the FWHM increases gradually with increasing refractive index. The contrast ratio tends to increase, but the trend is not serious. For the rough surface SPF, the FWHM of the normalized transmission curve increases to a greater extent with increasing refractive index, and this makes data fitting for obtaining the resonance wavelength more difficult, particularly for larger refractive indices. As such, the influence of surface topography on optical performance is clearly reflected in the resonance wavelength and the FWHM of the transmission spectrum.

To study the influence of oxidation on the optical performance of Ag-SPR sensors, all samples were immersed in standard index-matching fluids and transmission spectra were obtained at different times over a 192 h period. Fig. 10 presents the normalized transmission spectra of sample 1 in

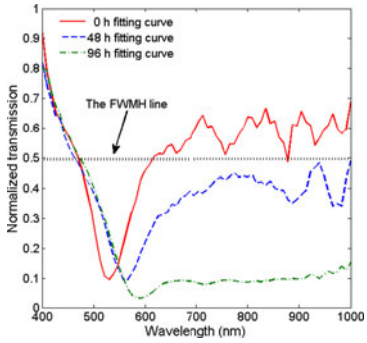

Fig. 10. Normalized transmission spectra of sample 1 in deionized water over 96 h.

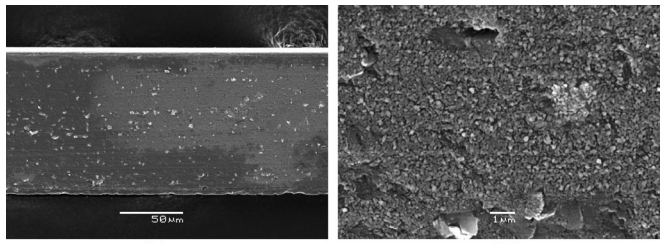

Fig. 11. Surface topography of Ag coating on sample 1 after 96 h.

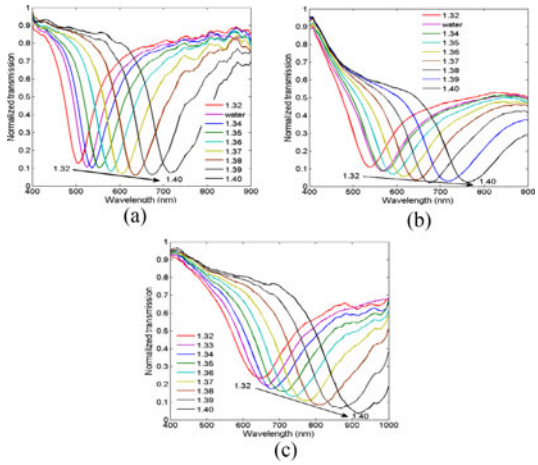

Fig. 12. Refractive index response of sample 2 over 192 h. (a) 48 h. (b) 96 h. (c) 192 h.

the refractive index medium of deionized water. The resonance wavelength exhibits a red shift with increasing time, which is similar to that observed with increasing refractive index, and the FWHM also exhibits considerable variation. The FWHM exceeds 500 nm after 48 h, and the contrast of the resonance dip nearly disappears after 96 h, which indicates a loss in the sensor's ability to detect the refractive index. Because the FWHM is still broadened for large refractive indices, the lifetime of sample 1 is less than 48 h. Fig. 11 presents SEM surface images of sample 1 after 96 h. Compared with Fig. 4(a), numerous flakes are observed on the surface of sample 1, which destroys the integrity of the Ag coating. These flakes also reveal that other physical mechanisms in addition to oxidation influence the optical performance of Ag-SPR sensors.

Fig. 12 presents the refractive index response curves of sample 2 over 192 h. The red shift of the resonance wavelength and the broadening of the FWHM are observed with increasing

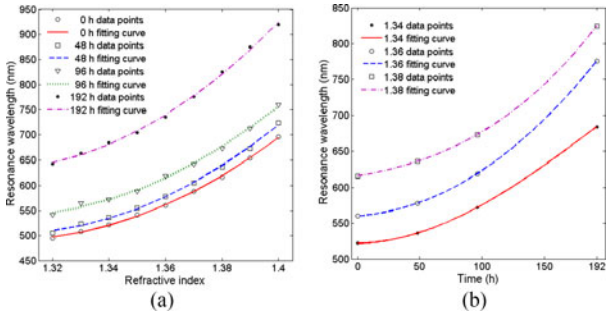

Fig. 13. Red shift of resonance wavelength for sample 2 over 192 h. (a) With respect to refractive index at different times. (b) With respect to time at a given refractive index.

refractive index at given times. In addition, the entire resonance band shifts to longer wavelength with increasing time, and the contrast of the resonance dip tends to decrease. By comparing Figs. 10 and 12, the smooth surface SPF exhibits retarded degeneration of the Ag film, and extends the lifetime of the Ag-SPF sensor. The surface topography determines the Ag-particle distribution on the SPF, which influences the adhesion and oxidation of the Ag coating significantly.

Fig. 13(a) represents the index of refraction sensitivity of sample 2 at different times. Fig. 13(b) shows the red shift of the resonance wavelength with time. The quick oxidation of Ag film weaken the resonance performance of outer electron and macroscopically change the average permittivity of the metal film. This may be the reason for the red shift of resonance wavelength with time. The sensitivity exhibits a quadratic relationship with the refractive index of the medium, and, for a given refractive index medium, the sensitivity does not change with time over the 192-h period. The maximum sensitivity is $\sim$4500 nm/RIU for a refractive index of $\sim$1.4. The degeneration of the Ag film affects only the resonance wavelength, but does not affect the sensitivity of the sensor. From Fig. 13(b), we find that the resonance wavelength shifts to longer wavelengths with increasing time, and, for a given refractive index medium, the rate of change in the red shift with respect to time is nearly equivalent to the extent of error. Although the Ag coating on the smooth polished surface degenerates rapidly, this degeneration does not influence the sensor sensitivity, and the small surface irregularity retards the rate of Ag degeneration compared with the rate of degeneration for the rough polished surface.

3.2 Inhibition of Ag Degeneration by Au Plating

Isolating the Ag coating from the environment is an effective method to inhibit the Ag-film degeneration, and to extend the Ag-SPF sensor lifetime. Gold plating is used to achieve this aim. The proportions of Ag and Au used in the experiments are listed in Table 2. Because the evaporation temperature of Au is greater than that of Ag, the Ag–Au compound layer structure can be obtained easily during a single course of evaporation. Fig. 14(a) and (b) presents the transmission spectra of samples 3 and 4, respectively, in different refractive index media (air and water). A comparison of the transmission curves in air with those in water shows the SPR resonance-absorption effect, but the influence of surface topography on the resonance wavelength and bandwidth is nearly eliminated. The contrast of the resonance dip, resonance wavelength, and the FWHM are nearly equivalent for the two samples, as shown in Fig. 14. Fig. 15(a) and (b) presents the normalized spectra of Fig. 14(a) and (b), respectively. The resonance wavelengths of samples 3 and 4 are 579 nm and 572 nm, respectively. Compared with the ideal position of 533 nm obtained for an ideal flat surface with a 45-nm-thick Ag coating, and the ideal position of 620 nm obtained for an ideal flat surface with a 45-nm-thick Au coating [14], the resonance dips of samples 3 and 4 are located near the middle of the ideal range between 533 nm and 620 nm. The FWHM of samples 3 and 4 are 158 nm and 160 nm, respectively, and are nearly equivalent. These findings show that the Ag–Au compound film decreases the influence of surface topography on the optical performance

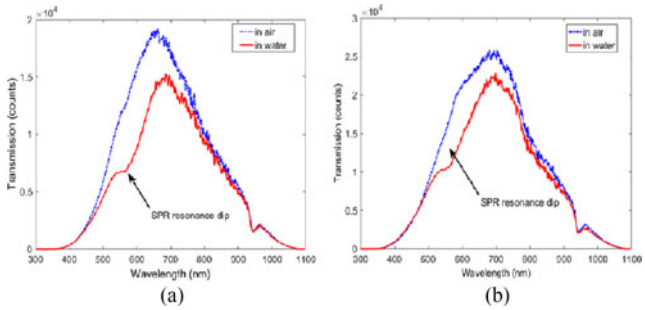

Fig. 14. Transmission spectra of SPF sensors with Ag-Au compound coatings. (a) Sample 3 (1500# abrasive paper). (b) Sample 4 (10000# abrasive paper)

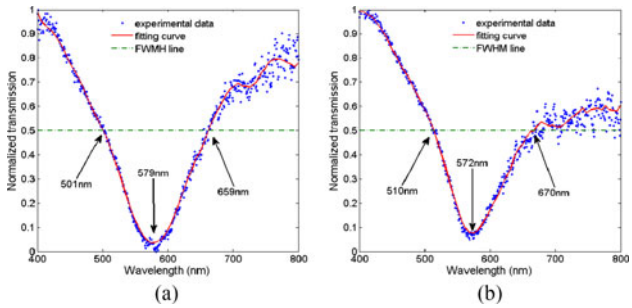

Fig. 15. Normalized transmission spectra of SPF sensors with Ag-Au compound coatings. (a) Sample 3 (1500# abrasive paper). (b) Sample 4 (10000# abrasive paper).

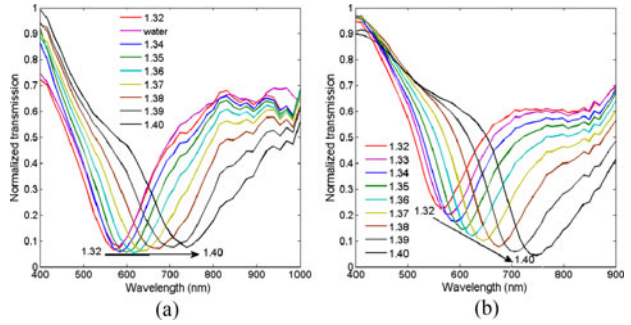

Fig. 16. Normalized transmission spectra of SPF sensors with Ag-Au compound coatings in different refractive index media. (a) Sample 3 (1500# abrasive paper). (b) Sample 4 (10000# abrasive paper).

of SPR sensors, and can be used to modify the position of the resonance wavelength by adjusting the proportions of Ag and Au.

Fig. 16(a) and (b) presents the refractive index responses of samples 3 and 4, respectively. For both samples, the resonance wavelength undergoes a red shift, and the FWHM increases gradually with increasing refractive index. The observed characteristics are similar to those observed for samples 1 and 2. In Fig. 16(a), deionized water replaced the refractive index medium of 1.34, and the water was not purged by alcohol prior to immersion into the refractive index medium of 1.32, which induced a large degree of error. Figs. 17 and 18 show the refractive index responses of samples 3 and 4, respectively, after 48 h, 96 h, and 192 h. The red shift of the resonance wavelength and the broadening of the FWHM are observed again with increasing refractive index at given times, and the overall resonance bands shift to longer wavelengths with increasing time. Compared with Fig. 12, the maximum resonance wavelength remains less than 900 nm, and the rate of change in

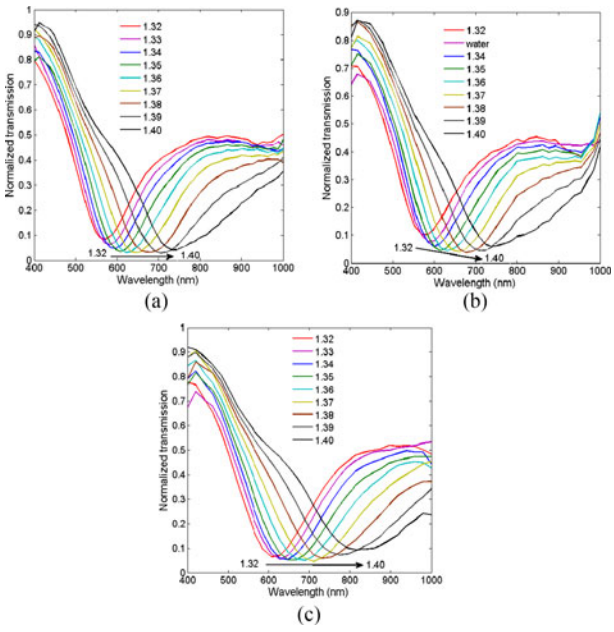

Fig. 17. Refractive index response of sample 3 over 192 h. (a) 48 h. (b) 96 h; (c) 192 h.

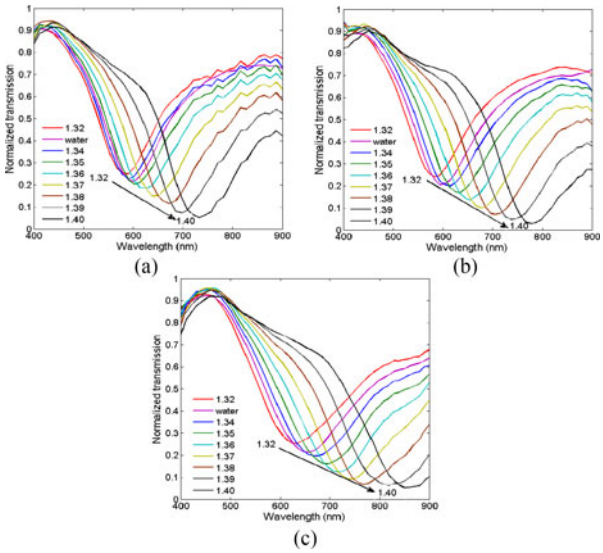

Fig. 18. Refractive index response of sample 4 over 192 h. (a) 48 h. (b) 96 h. (c) 192 h.

the red shift of the resonance wavelength with respect to time appears to be less than that of the pure Ag-SPF sensor.

Fig. 19(a) and (b) represents the index of refraction sensitivity of samples 3 and 4 at different times, respectively. The observed relationships between the sensitivity and the refractive index are similar to that observed for sample 2. The maximum sensitivities of samples 3 and 4 are ∼4200 nm/RIU and 4700 nm/RIU, respectively, and were observed at a refractive index of ∼1.4. The average value of 4500 nm/RIU is equivalent to that of sample 2. However, the rate of change in the red shift with respect to time for samples 3 and 4, which here exhibit an increase, a decrease, and then an increase, is different from that of sample 2, which exhibits only an increasing rate of change. The first period of increase may result because of the rapid reaction or diffusion (physical

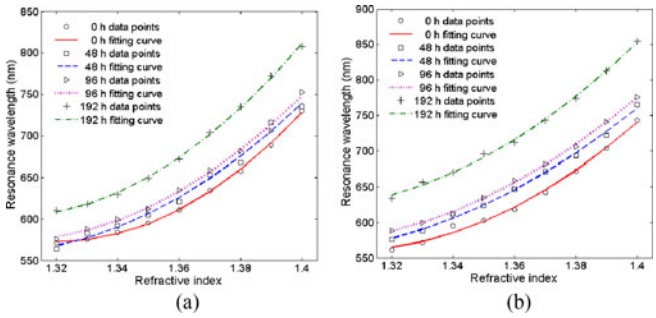

Fig. 19. Index of refraction sensitivity at different times. (a) Sample 3 (1500# abrasive). (b) Sample 4 (10000# abrasive).

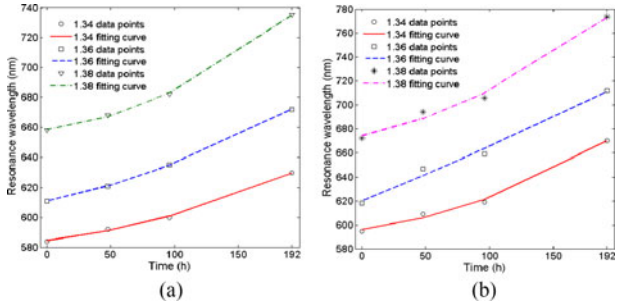

Fig. 20. Red shift of resonance wavelength with respect to time. (a) Sample 3 (1500# abrasive). (b) Sample 4 (10000# abrasive).

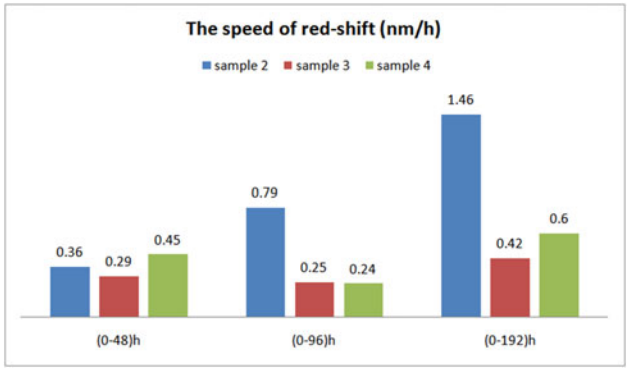

Fig. 21. Inhibition effect of Au plating on Ag degeneration.

or chemical) of the Ag and Au particles. Fig. 20(a) and (b) shows the red shift of the resonance wavelength with respect to time for samples 3 and 4, respectively, for different refractive index media. Compared with Fig. 13(b), the resonance wavelength shifts to longer wavelengths with increasing time, but the rate of change is less than that observed for sample 2. The behavior conforms to a linear relationship rather than to a quadratic relationship as exhibited by sample 2. Although the Ag coating still degenerates under the Au plating, the rate of change in the red shift of the resonance wavelength with respect to time decreases relative to that of the pure Ag film, and this reveals that the Au plating retards the rate of Ag degeneration. The Au plating also decreases the SPR bandwidth of the rough surface, and extends the service lifetime of the sensor.

Fig. 21 presents the rates of change in the red shift of the resonance wavelength with respect to time for samples 2, 3, and 4 during different time periods based on the average values of the data given in Figs. 13(b) and 20. Fig. 21 indicates that the rate of change in the red shift

can reflect the degeneration rate of the Ag film indirectly. The rate of degeneration for sample 2 increases continuously over the three time periods considered, whereas the rates of degeneration for samples 3 and 4 first decrease, and then increase. This corresponds with the behaviors observed in Figs. 13(a) and 19. The rate of degeneration differs little between the three samples over the first 48 h. However, during the second and third time periods, the rate of change in the red shift with respect to time for sample 2 is greater than that of samples 3 and 4, particularly between 96 h and 192 h, and the maximum rate of Ag degeneration for the pure Ag coating is 3.5 times greater than that of the Ag–Au compound coatings. The inhibition of Ag degradation by Au plating is visible in Fig. 21.

4. Conclusion

This research evaluated experimentally the degeneration of Ag coatings on different polished surfaces of SPFs, and the inhibition effect of Au plating. The results of the experiments demonstrate the following.

1) A fine abrasive tends to remove SiO_2 by a plastic mechanism with little debris and minor pitting on the polished surface, and a coarse abrasive is likely to yield a brittle surface with numerous fractures and scratches. The resonance wavelength for the rough and smooth surfaces exhibits a red shift over time. However, the service lifetime of the Ag-SPF sensor with a rough surface was less than 48 h because the numerous flakes destroy the integrity of the Ag coating. For the smooth surface, the maximum index of refraction sensitivity was $\sim$4500 nm/RIU, which occurred at a refractive index of $\sim$1.4. Although the Ag coating on the smooth polished surface still degenerated rapidly, the degeneration did not influence its sensitivity, and the small surface irregularity retarded the rate of Ag degeneration compared with that of the rough surface.
2) Thin Au plating eliminates the influence of surface topography on the resonance wavelength and bandwidth, and provides a resonance wavelength near the middle of the ideal range (between 533 nm and 620 nm). This behavior reveals that the Ag–Au compound coating can be used to modify the position of the resonance wavelength by adjusting the proportions of Ag and Au. Although the Ag coating under the Au plating still degenerates, the rate of change in the red shift of the resonance wavelength with respect to time decreased. This reveals that the Au plating retards the rate of Ag degeneration. In addition, the Au plating also decreases the SPR bandwidth of the rough surface significantly, and extends the sensor service lifetime. The maximum rate of degeneration for the pure Ag coating was 3.5 times greater than that of the Ag–Au compound coating between 96 h and 192 h.

References

[1] A. Otto, "Exitation of nonradiative surface plasma waves in silver by the method of frustrated total reflection," *Z. Phys.*, vol. 216, pp. 398–410, 1968.
[2] E. Kretchmann, "Die bestimmung optischer konstanten von metallen durch anregung von oberflachenplasmashwingungen," *Z. Phys.*, vol. 241, pp. 313–324, 1971.
[3] H. Raether, *Surface Plasmons on Smooth and Rough Surfaces and on Gratings* (Volume 111 of Springer Tracts in Modern Physics). Berlin, Germany: Springer, 1988, pp. 1–135.
[4] T. Murao, K. Saitoh, and M. Koshiba, "Design of air-guiding modified honeycomb photonic band-gap fibers for effectively single mode operation," *Opt. Exp.*, vol. 14, pp. 2404–2412, 2006.
[5] M. Hautakorpi, M. Mattinen, and H. Ludvigsen, "Surface-plasmon-resonance sensor based on three-hole microstructured optical fiber," *Opt. Exp.*, vol. 16, pp. 8427–8432, 2008.
[6] Q. L. Bao *et al.*, "Broadband graphene polarizer," *Nature Photon.*, vol. 5, pp. 411–415, 2011.
[7] Y. L. Lo, C. H. Chuang, and Z. W. Lin, "Ultrahigh sensitivity polarimetric strain sensor based upon D-shaped optical fiber and surface plasmon resonance technology," *Opt. Lett.*, vol. 36, pp. 2489–2491, 2011.
[8] J. Koo and J. H. Lee, "Passive Q-switching of a fiber laser using a side-polished birefringent fiber with index matching gel spread on the flat side," *Appl. Phys. B*, vol. 112, pp. 61–65, 2013.
[9] Y. J. He, "Novel D-shape LSPR fiber sensor based on nano-metal strips," *Opt. Exp.*, vol. 21, pp. 23498–23510, 2013.
[10] J. Zhao *et al.*, "Rough side-polished fiber with surface scratches for sensing applications," *IEEE Photon. J.*, vol. 7, no. 3, Jun. 2015, Art. no. 6801107.

[11] J. A. Kim, "Graphene based fiber optic surface plasmon resonance for bio-chemical sensor applications," *Sensors Actuators B, Chem.*, vol. 187, pp. 426–433, 2013.
[12] R. Verma, and B. D. Gupta, "Detection of heavy metal ions in contaminated water by surface plasmon resonance based optical fibre sensor using conducting polymer and chitosan," *Food Chem.*, vol. 166, pp. 568–575, 2015.
[13] J. M. J. Santillán, L. B. Scaffardi, and D. C. Schinca, "Determination of nanometric Ag2O film thickness by surface plasmon resonance and optical waveguide mode coupling techniques," *J. Opt.*, vol. 12, no. 4, 2010, Art. no. 045002.
[14] G. Wang *et al.*, "Side-opened suspended core fiber-based surface plasmon resonance sensor," *IEEE Sensors J.*, vol. 15, no. 7, pp. 4086–4092, Jul. 2015.